Available online at www.sciencedirect.com
ScienceDirect
Biochimica et Biophysica Acta 1778 (2008) 79–87
Biochimica et Biophysica Acta
BBA
www.elsevier.com/locate/bbamem

Positional dependence of non-native polar mutations on folding of CFTR helical hairpins

Hania Wehbi [a,b,1], Geneviève Gasmi-Seabrook [a,1], Mei Y. Choi [a,b], Charles M. Deber [a,b,*]

[a] Division of Molecular Structure and Function, Research Institute, The Hospital for Sick Children, Toronto, Ontario, Canada M5G 1X8
[b] Department of Biochemistry, University of Toronto, Toronto, Ontario, Canada M5S 1A8

Received 6 July 2007; received in revised form 27 August 2007; accepted 29 August 2007
Available online 15 September 2007

Abstract

Mutations of the cystic fibrosis transmembrane conductance regulator (CFTR) cause CF disease by altering the biosynthesis, maturation, folding and ion conductance of this protein. Our laboratory has focused on expression and structural analysis of the CFTR transmembrane (TM) domains using two-TM segments (i.e., helix–loop–helix constructs) which we term 'helical hairpins'; these represent the minimal model of tertiary contacts between two helices in a membrane. Previous studies on a library of TM3/4 hairpins of the first CFTR TM domain suggested that introduction of non-native polar residues into TM4 can compromise CFTR function through side chain-side chain H-bonding interactions with native Q207 in TM3 [Choi, M. Y., Cardarelli, L., Therien, A. G., and Deber, C. M. Non-native interhelical hydrogen bonds in the cystic fibrosis transmembrane conductance regulator domain modulated by polar mutations, Biochemistry 43 (2004) 8077–8083]. In the present work, we combine gel shift assays with a series of NMR experiments for comparative structural characterization of the wild type TM3/4 hairpin and its mutants V232D, I231D, Q207N/V232E. Over 95% of the backbone resonances of a ^{15}N,^{13}C-labelled V232D-TM3/4 construct in the membrane-mimetic environment of perfluorooctanoate (PFO) micelles were successfully assigned, and the presence and boundaries of helical segments within TM3 and TM4 were defined under these conditions. Comparative analysis of ^{15}N and ^{1}H chemical shift variations among HSQC spectra of WT-, V232D-, I231D- and Q207N/V232E-TM3/4 indicated that hairpin conformations vary with the position of a polar mutation (i.e., V232D and I231D vs. WT), but remain similar when hairpins with identically-positioned polar partners are compared (i.e., V232D vs. Q207N-V232E). The overall findings suggest that a polar mutation in a TM helix can potentially distort native interfacial packing determinants in membrane proteins such as CFTR, with consequences that may lead to disease.

Keywords: CFTR; Transmembrane segment; Helical hairpin; NMR spectroscopy; Membrane protein; Helix–helix interaction

1. Introduction

Cystic Fibrosis (CF) is the most prevalent genetic disease among Caucasians, affecting one out of 2500 newborns [1]. Numerous phenotypes associated with CF include increased sweat chloride concentration, protein aggregation in the pancreas and subsequent blockage of the ductal system [2], male infertility [3], and mucus accumulation in the lungs. The latter constitutes the most life-threatening feature of cystic fibrosis, especially with the subsequent colonization of the lungs by *Pseudomonas aeruginosa* [4]. The gene defective in CF codes for a cAMP-dependent chloride channel, the cystic fibrosis transmembrane conductance regulator, CFTR, present at the apical border of epithelial cells [5,6]. CF is inherited in a recessive autosomal fashion; most CF patients have a CFTR

Abbreviations: CF, Cystic fibrosis; CFTR, Cystic fibrosis transmembrane conductance regulator; TM, Transmembrane; TMD, Transmembrane domain; TM3/4, Helical hairpin including residues 194–241 of CFTR; WT, Wild type; V232D-TM3/4, TM3/4 construct with mutation of Val to Asp at position 232; I231D-TM3/4, TM3/4 construct with mutation of Ile to Asp at position 231; Q207N/V232E-TM3/4, TM3/4 construct with mutation of Gln to Asn at position 207 and Val to Glu at position 232; PFO, Perfluorooctanoate; DPC, Dodecylphosphocholine; SDS, Sodium dodecylsulfate; CD, Circular dichroism; H-bond, Hydrogen bond; HSQC, Heteronuclear single quantum coherence

* Corresponding author. Division of Molecular Structure and Function, Research Institute, Hospital for Sick Children, 555 University Avenue, Toronto, Ontario, Canada M5G 1X8.
E-mail address: deber@sickkids.ca (C.M. Deber).
[1] These authors contributed equally to this work.

0005-2736/$ - see front matter © 2007 Elsevier B.V. All rights reserved.
doi:10.1016/j.bbamem.2007.08.036

gene deletion of three base pairs, ΔF508, but over 1300 other CF causing mutations have been found worldwide [7]. In addition to its primary function in chloride conductance, CFTR has been shown to play a role in regulating the function of other ion channels such as the amiloride sensitive epithelial sodium channel (EnaC) [8] and the outwardly rectifying chloride channel (ORCC) [9].

CFTR belongs to the ATP-binding cassette transporter superfamily [6]. The protein contains 1,480 residues divided into two homologous halves, each consisting of a transmembrane (TM) domain and a nucleotide-binding domain. CFTR also has a so-called R domain, unique to CFTR, known to regulate the channel activity through phosphorylation [10]. Each of the two TM domains is predicted to be composed of six TM helices [6]. Assessment of the ion conductance of the first TM domain (TMD1, helices 1–6) showed that this domain is sufficient to produce an active chloride channel [11], and residues in TM6 of this domain involved in anion–cation selectivity and permeation properties of the channel were determined [12,13]. Fewer studies of the structural and functional details of TMD2 of CFTR are available to-date; it has been shown to form a dimer in micellar environments and exhibits channel function under these conditions [14]. However, a full understanding of how CFTR functions, and how the TM segments within each domain interact and induce long range communication leading to ion conductance, remains to be achieved.

CFTR presents a vivid example of the connection of membrane proteins to occurrence of disease [15]. Out of approximately 1500 CF-causing mutations now known for this protein, nearly 200 are present in the TM domains [7]. While one would prefer to perform structural investigations on intact CFTR, the facts that (i) the protein cannot be readily expressed in preparative amounts; and (ii) the local structural effects of point mutations in the 1480-residue protein may fall below detection by spectroscopic analysis, have greatly limited biophysical studies on the full-length molecule. As well, TM segments have been shown to behave as independent folding domains even when excised from the protein, and to retain the native contacts that they exhibit within the intact protein [16–18]. These realities have encouraged us and others to develop the use of defined domain constructs of CFTR that can be manipulated by established biophysical techniques, and can be used to characterize the molecular events that link CF disease to CF-phenotypic mutations. Our laboratory has focused on expression and structural analysis of the CFTR transmembrane domains using two-TM segments (i.e., helix–loop–helix constructs) which we term 'helical hairpins'; these represent the minimal model of tertiary contacts between two helices in a membrane. We have expressed two-helix constructs of several portions of the CFTR TMD1 in milligram quantities, and have been engaged in biophysical investigations on wild type and CF-phenotypic mutant libraries of these proteins, including TM1/2 [19]; TM3/4 [20–22]; and TM5/6 [23] (notation: TM1/2 = TM1 helix + intervening loop + TM2 helix, etc.). The latter work has been further catalyzed by the observations that (i) single TM segments of integral proteins form helical structures in membrane-mimetic environments [24–26]; and (ii) the assembly of co-expressed or synthesized fragments of several membrane proteins generated functional properties comparable to the intact protein [27–32].

Previous studies we performed on CFTR helix–loop–helix constructs using gel shift analysis, fluorescence measurements, and molecular modeling suggested that hairpin folding is likely stabilized by folding due to formation of a non-native side chain-side chain hydrogen bond between 'polar partners' in the interacting helices (*viz*., Q207 in TM3, and I231D or V232D in TM4) [20]. Such non-native interactions can interfere with the normal assembly and the alignment of TM helices of CFTR, altering channel function, thus causing CF [20]. However, these studies cannot provide direct structural information as to how/if the position of the non-native polar site influences hairpin folding. Since protocols have become available to routinely produce milligram amounts of helix–loop–helix fragments from CFTR TMD1 in minimal media [19], NMR experiments on these hairpins in membrane environments became an option. However, while membrane proteins constitute about 30% of the genomes of various organisms [33], only a small number of the solved structures deposited in the protein data bank belong to membrane proteins. This situation arises, in part, because solution NMR spectroscopy – one of the most powerful techniques for protein structural determination – is subject to line broadening caused by the large size of the membrane protein–micelle complexes and to the small proton chemical shift dispersion (~1.4 ppm), consequently leading to resonance overlaps. Notwithstanding these inherent challenges, a number of structures of membrane proteins and fragments of helical [29–38] and β-barrel [39–42] membrane proteins have been successfully characterized using solution NMR spectroscopy. Here we have performed a series of gel electrophoresis experiments that illustrate the responsiveness of the migration rate of CFTR membrane domain segments to position and type of polar TM mutations. We then use solution NMR experiments to demonstrate the conformational variability of TM3/4 hairpin mutants (including the CF-phenotypic mutant V232D; I231D; and Q207N/V232E) vs. the wild type hairpin in micellar environments.

2. Materials and methods

2.1. Expression and purification of wild type and mutant TM3/4 constructs from the CFTR membrane domain

The ^{15}N and $^{15}N/^{13}C$ enriched forms of the TM3/4 helical hairpin constructs (WT-, V232D-, I231D-, Q207N/V232E) were expressed and purified as previously described [19]. In each of these constructs, wild type Cys225 was changed to an Ala to avoid disulfide bond formation between different helical hairpin molecules. cDNA encoding for residues 194 to 241 (TM segments 3 and 4) of CFTR was subcloned into PET-32a. This construct also contains a fusion protein (thioredoxin) to aid in solubilizing the hydrophobic CFTR fragment, an S-tag that allows detection of TM3/4 by Western blot, and a His-tag for purification purposes. TM3/4 mutants were obtained using Stratagene's QuikChange site-directed mutagenesis kit. The resulting constructs were transformed into BL-21 cells in M9 medium (M9 salts: 0.8% Na_2HPO_4 (w/v), 0.4% KH_2PO_4 (w/v), 0.05% NaCl (w/v), and 0.1% $^{15}NH_4Cl$ (purchased from Cambridge Isotope Laboratories) in 1 L water, pH adjusted to 7.5). Prior to cell growth, the medium was supplemented with biotin and thiamine (1 mg/L of each); sterile $MgSO_4$ and $CaCl_2$ stock solutions to final concentrations of 1 mM and 0.3 mM, respectively; 3 g of glucose for expression of ^{15}N isotopically labeled V232D-TM3/4, or ^{13}C

glucose (purchased from Cambridge Isotope Laboratories) for expression of $^{15}N/^{13}C$ isotopically labeled TM3/4; and 100 μg/mL ampicillin. The cells were grown at 37 °C and induced at an O.D. of 0.6 with 0.1 mM IPTG, followed by overnight shaking at room temperature. Harvested cells were sonicated in 20 mM Tris, pH 8.0, and then centrifuged. The soluble fraction was supplemented with NaCl (150 mM), β-mercaptoethanol (20 mM), imidazole (5 mM), and 0.1% Triton X-100, and then applied to a nickel affinity resin (from Qiagen) pre-equilibrated under the same conditions as the protein mixture, and binding was allowed to proceed overnight at room temperature. Elution was performed with the same equilibration buffer containing 400 mM imidazole. Eluted fractions were then treated with $CaCl_2$ (5 mM) and thrombin (15 U). Thrombin-treated TM3/4 was purified by RP-HPLC on a C4 semipreparative column (Phenomenex) using an isopropanol gradient. Protein-containing fractions were obtained by monitoring A_{215}, and evaporated under nitrogen until they contained less than 20% isopropanol. The resulting fractions were then lyophilized. The yield was ca. 10 mg of TM3/4 (>95% pure) per 1 L of minimal M9 medium. The sequence of the WT-TM3/4 construct obtained in this manner is GSGMKETAAAK-FERQHMDSPDLGTDDDDKAMGLALAHFVWIAPLQVALLMGLIWELLQ-ASAFAGLGFLIV^{232}LALFQAGLGLEHHHHHH with residues 194–241 of CFTR (TM3/4) in bold. The site of CF-phenotypic mutation at Val-232 is indicated. Residues in the TM3/4 segment were numbered according to their position in full-length CFTR (194–241). The S-tag and the His-tag are at the N-terminal and C-terminal end, respectively. Residues in the N-terminal tag region were numbered 1 to 31 and at the C-terminus numbered as 32 to 39.

2.2. PAGE analysis

The dry protein samples were resuspended in NuPage SDS sample buffer and 1 μg of each protein run on 12% NuPAGE Bis-Tris gels with MES running buffer. Gels were stained with Coomassie Blue (according to standard protocols) for analysis.

2.3. NMR Spectroscopy

Spectra were recorded in various detergents [285 mM (10%) DPC, 115 mM (5%) PFO, and 175 mM (5%) SDS], at several temperatures (30 °C, 37 °C, 45 °C), on four channel Varian Inova 500 and 600 MHz spectrometers equipped with z-axis pulsed field gradient units and room-temperature shielded triple resonance probes. NMR sample concentrations were about 1 mM of ^{15}N labeled TM3/4 in the given detergent, 10% D_2O, and 50 mM sodium phosphate, pH 6.5. Triple resonance NMR experiments for $^{15}N/^{13}C$ isotopically enriched V232D-TM3/4 115 mM PFO were carried out at 45 °C. For backbone assignments, three triple-resonance experiments were performed: HNCACB [43], CBCA(CO)NH [44], and HNCO [45]. For side-chain assignments, both 3D (H)CC(CO)NH-TOCSY [46] and 3D H(CC)(CO)NH-TOCSY [47] experiments were performed. A mixing time of 100 ms was used in the 3D simultaneous $^{15}N,^{13}C$-edited NOESY [48] experiment. The programs NMRPipe [49] and NMRVIEW [50] were used to process and analyze the data. TALOS was used to predict the ϕ/ψ backbone dihedral angles based on comparison of the NMR chemical shifts and sequence homology of TM3/4 with a database [51].

2.4. Circular dichroism spectroscopy

CD spectra of TM3/4 were measured on samples of *ca*. 1 mM TM3/4 (WT or mutants) in 5% PFO and 50 mM sodium phosphate, pH 6.5) using a cell with 1 mm path length at room temperature on a Jasco J-720 CD spectrometer.

3. Results

Various hydropathy algorithms have been previously employed to predict the membrane topology of the TM domains of CFTR [6,24]. Here we used *TM Finder* [52] to refine the boundaries of the helical segments of TM3 and TM4 of CFTR. *TM Finder* predicted an extended TM helix stretch between 197 and 240 that displays reduced helicity/hydrophobicity around residues 216–226 (WELLQASAFAG), which is the maximum region through which the extracellular loop between helix 3 and 4 would most likely occur [52]. Based on the limits of TM3 and TM4 determined from prediction by *TM Finder*, residues 194 to 241 were selected as boundaries for the TM3/4 helical hairpin constructs employed in our studies (see Materials and methods). Given the limited number of residues in the turn connecting TM3 and TM4 in the CFTR TMD1, it is likely that these two helices will be in contact in the native protein. Following successful expression of the desired constructs in *Escherichia coli* cells, we initially assessed their migration properties on SDS-PAGE gels.

3.1. Helical hairpins of the transmembrane domain of CFTR

Sodium dodecylsulfate-polyacrylamide gel electrophoresis (SDS-PAGE) "gel-shift assays" have been shown to be useful in detecting differences in interhelical packing caused by CF-phenotypic mutants that occur within the TM helices themselves [20,22]. In this earlier work, it was observed that the more compact hairpins ('closed' conformation) migrate *faster* than the corresponding elongated ('open' or more rod-like) form of the protein, with migration differences interpreted principally in terms of the strength of proposed side chain-side chain interhelical H-bonds [20–22]. The assay is quite sensitive, and deviations from wild type migration of as much as 30–40% from the actual molecular weight position arise from single point mutations in an otherwise identical protein [22,53]. Thus, prior to our NMR studies, we initially applied this assay to a series of TM3/4 mutants to determine their responsiveness to introduction/deletion of selected polar residues (Fig. 1a, b). The sensitivity of the assay is illustrated in Fig. 1a. Here, the double mutant Q207N/V232E migrates significantly faster than wild type, indicating that the N/E pair is likely involved in side chain-side chain interactions analogously to the Q/D pair at the corresponding positions in the TM3/4-V232D single mutant [22]. In contrast, replacement of wild type Q237 in TM4 with the non-polar Leu residue (mutant Q237L) creates a *slower* migrating hairpin vs. wild type (Fig. 1a), suggesting that some pre-existing inter-helical interactions – conceivably attributable to a network of H-bonding interactions – have been removed. The helix–helix interactions influenced by polar mutants among the positions studied are summarized in Fig. 1b, where it is seen that constructs involving I231 and V232 with combinations of TM4 D-mutations, as well as various combinations of Q207N with D and E mutants in TM4, migrate between 7 and 20% faster than the WT construct. From these, we selected three mutants (indicated by white dots on the bar graphs) for comparative structural analysis by NMR spectroscopy.

3.2. Chemical shift assignment and secondary structure analysis of V232D-TM3/4 in PFO

$^{1}H–^{15}N$ HSQC spectrum of ^{15}N-enriched V232D-TM3/4 in 115 mM PFO at 45 °C is shown in Fig. 2. The best amide dispersion was obtained under these conditions, in comparison to parallel determinations performed in 285 mM DPC and 175 mM SDS. In PFO with *ca*. 1 mM protein, the molar ratio of

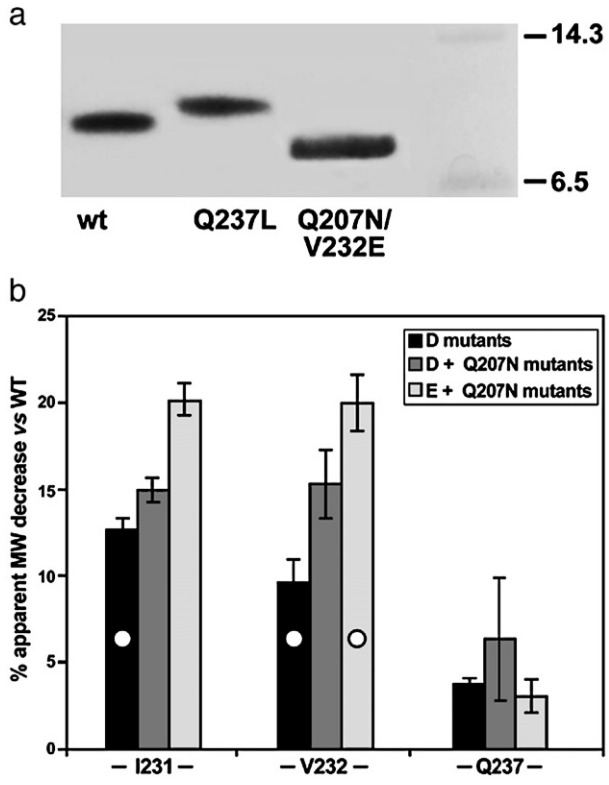

Fig. 1. SDS-PAGE gels of CFTR TM3/4 helical hairpins. (a) Relative migration rates of wild type CFTR TM3/4 and mutants Q237L and Q207N-V232E. Molecular weight markers are shown in the right lane. (b) Gel shift (SDS-PAGE) analysis of D, D+Q207N, and E+Q207N mutant migration rates at positions I231, V232, and Q237 vs. wild type in CFTR TM3/4 constructs. Taller bars indicate relative faster migration, and hence correspond to a might tightly folded hairpin. Note that the vertical axis is given as "% apparent MW decrease" such that the actual band appearance of all these mutants on gels is similar to Q207N-V232E in (A), i.e., faster migration than wild type. Mutants specifically studied in this work are indicated by white circles on their respective bars.

PFO/protein = 100, which in principle computes to one protein/4–5 PFO micelles [54]. HSQC spectra were reproducible, and the sample was stable under these conditions over the course of data acquisition, with no discernible aggregation or visible protein precipitate. CD spectroscopy performed using the NMR sample directly (*ca*. 1 mM protein in PFO/buffer) gave a spectrum indicating a pattern indicating high helical content for this construct typical of that expected for the protein in a membrane environment, although the ellipticity was damped due to the high protein concentration and PFO background absorption (data not shown).

Analysis of the triple resonance experiments HNCACB, CBCA(CO)NH, HNCO, (H)CC(CO)NH-TOCSY, and H(CC)(CO)NH-TOCSY of the ^{15}N,^{13}C-labeled V232D-TM3/4 enabled the assignments for 95% of the residues in the TM3/4 region, despite the fact that the analysis was complicated due to crosspeak overlapping typical of native helical TM proteins in detergent micelles. The amide assignments obtained are labelled on the ^{1}H–^{15}N HSQC spectrum shown in Fig. 2. The $^{13}C_{\alpha}$, $^{13}C_{\beta}$, CO chemical shift deviation from "random coil" values, the slow amide proton exchange with water in conjunction with the NOE pattern strongly indicate the presence of two helices (Fig. 3). H_{α}, C_{α}, C_{β}, CO, and N^{H} chemical shifts of V232D-TM3/4 residues were analyzed using TALOS [51]. The secondary structure elements of V232D-TM3/4 thus obtained agree broadly with the formation of two helices in the micelle environment, separated by a turn. The chemical shift deviation along with the amide ^{1}H exchange and NOE patterns, further suggest a discontinuity in secondary structure in TM3 localized around P205; these residues do not present any of the features (chemical shift deviation, NOE patterns and amide proton exchange) of amino acids that are part of a helix (Fig. 3). The amide peak intensities of I203 and V208 on either side of P205 have intensities close to the noise level in the ^{1}H–^{15}N HSQC of TM3, likely indicating some intermediate exchange attributable to local protein dynamics. We further noted that Q207 and Q237 side chain carboxamide protons did not exchange with water, and one of the two Q220 protons was in slow exchange; Q15 protons (in the S-tag) exchanged rapidly with water.

The 3D simultaneous ^{15}N,^{13}C-edited NOESY spectrum was recorded with a mixing time of 100 ms. The short- and medium-range NOEs observed in the spectra are consistent with the presence of helical secondary structure. Most of the long-range NOEs that were observed could not be specifically assigned due to the high occurrence of Leu and Ile residues in both TM helices. Few long-range NOEs were observed within the TM3–TM4 turn region: the S222 amide showed a weak NOE with protons from the aromatic ring of F224, as well as with the methyl groups of L218 or L219. The amides of A223 and F224 also showed weak NOEs with the methyl groups of L218 or L219 and L227.

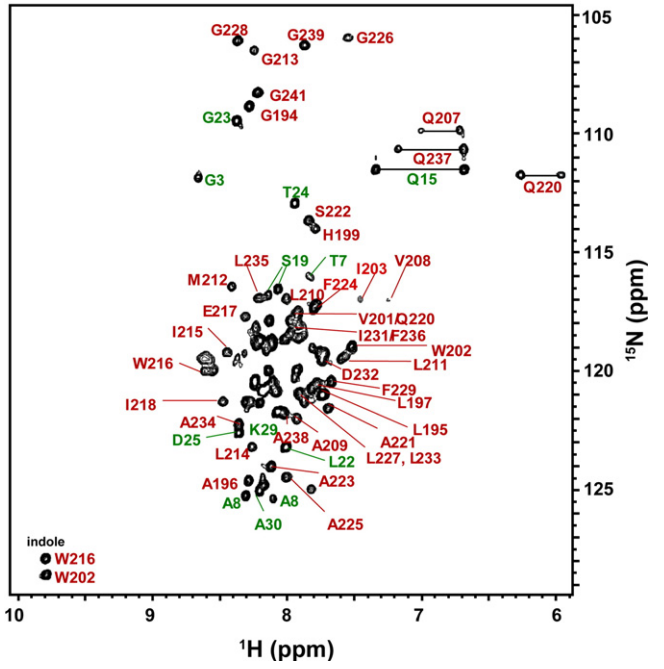

Fig. 2. ^{1}H–^{15}N HSQC spectrum of ^{15}N-labeled TM3/4 mutant V232D with amide chemical shift assignments. The spectrum was recorded in 115 mM (5%) PFO micelles. The red-labeled amino acids correspond to the residues present in the TM3/4 segment of the construct; those displayed in green are from residues present in the S-tag and His-tag regions. Data were acquired on Varian Inova 600-MHz spectrometer at 45 °C.

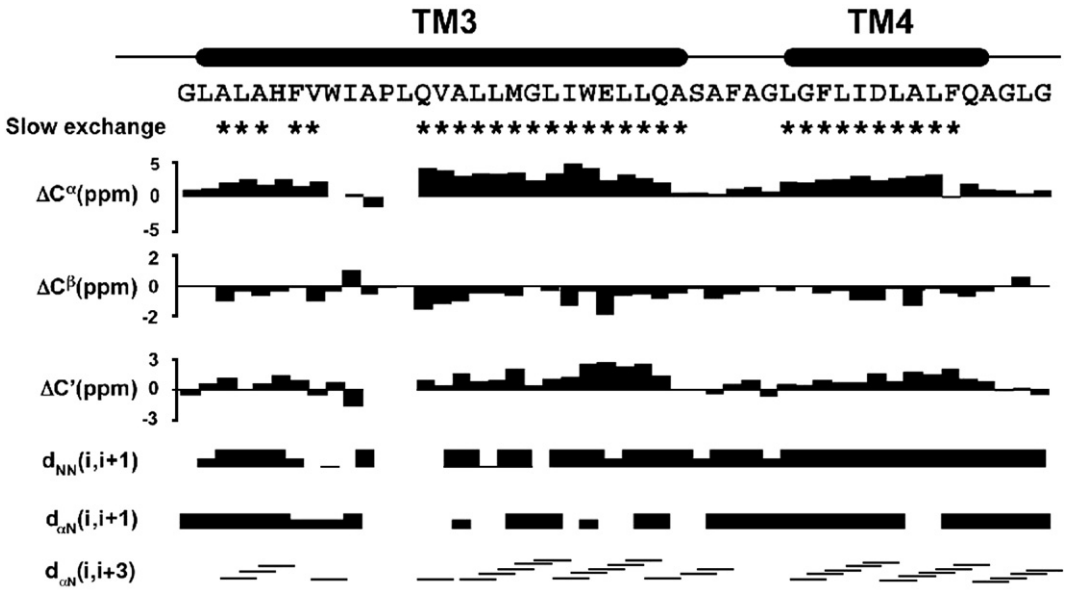

Fig. 3. Summary of the chemical shift deviation and the sequential, mid-range NOEs for V232D-TM3/4 in PFO micelles. The chemical shift deviation was determined on the basis of the chemical shift differences between the random coil and the TM3/4 C^{α}, C^{β} and carbonyl values. Residues exhibiting slow amide proton (from ^{15}N–^{13}C-edited NOESY) exchange are indicated by asterisks. The thickness of the lines is proportional to the NOE intensities. TM3/4 α-helical structure elements are displayed above the amino acid sequence.

However, these NOEs were not sufficient *per se* for calculation of a defined tertiary structure for the V232D-TM3/4 hairpin.

3.3. Analysis of ^{1}H–^{15}N HSQC spectra of WT-TM3/4 and its various mutants in PFO micelles

To probe for global conformational changes of TM3/4 upon introducing a polar residue in TM4, the ^{1}H–^{15}N HSQC spectrum of wild type CFTR TM3/4 was acquired in PFO micelles under the same buffer conditions as V232D-TM3/4. With the amide chemical shift assignments of V232D-TM3/4 in hand, and because these two constructs differ by only a single residue, any major differences in the ^{1}H–^{15}N HSQC spectra should be attributable to the modification of the electrostatic environment by the non-polar-to-polar residue mutation at position 232, as well as to any resulting conformational changes.

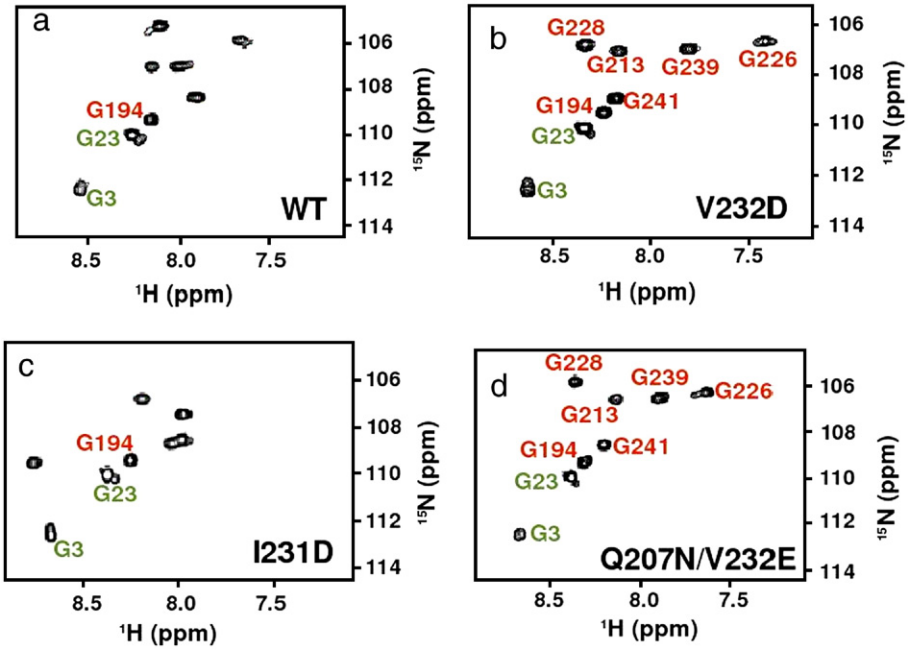

Fig. 4. The "Gly box" region of the ^{1}H–^{15}N HSQC spectra, containing resonances of the eight Gly residues present in each CFTR TM3/4 construct. (a) WT; (b) V232D; (c) I231D; and (d) Q207N/V232E. Spectra were recorded in 115 mM PFO at 45 °C. Gly cross-peaks (shown in (b)) were assigned from the V232D spectrum (Fig. 2); other assignments shown were made where possible by comparison.

To simplify the comparison between the two spectra, we focused our analysis on the glycine cross-peaks, noting that several of the Gly residues occur within TM helical regions (Fig. 4). As illustrated in the 'Gly box', $^{1}H–^{15}N$ HSQC spectra of WT-TM3/4 (Fig. 4a) and V232D-TM3/4 (Fig. 4b) do possess some similarities. We first noted that G3 and G23 (present in the S-tag region), and G194 (in the N-terminus of TM3) did not display any chemical shift changes and could be assigned by analogy. However, among the four spectra shown, significant chemical shift changes are observed for several of G213, G226, G228, G239 and G241 resonances between WT and V232D-TM3/4. As assignments were available only for the V232D-TM3/4 construct, we could not assign the full complement of WT Gly resonances specifically; however, the observed shifts are suggestive of a change of the environment of these residues. The shift changes observed in the Gly-box – and indeed throughout the entire protein – very likely reflect the differences in relative arrangements of the helices, as well as some local effects due to the introduction of a negative charge.

In order to further investigate the conformational changes of TM3/4 upon introduction of a polar residue into TM4, we next performed a comparative analysis of amide $^{1}H/^{15}N$ chemical shifts in the $^{1}H–^{15}N$ HSQC spectra of WT-TM3/4 vs. I231D-TM3/4 which contains a polar mutation at the position preceding the CF-phenotypic mutation V232D-TM3/4. Note that this mutant exhibited a faster migration rate than both WT-TM3/4 and V232D-TM3/4 on SDS-PAGE [22] (Fig. 1b). From the analysis of the Gly cross-peaks (Fig. 4c), one observes that the N–H chemical shifts of G3, G23, and G194 remain identical to the WT, but obvious changes occurred for G213, G226, G228, G239 and G241 to the extent that we could not formally assign them by comparison To V232D-TM3/4. These data, together with SDS-PAGE results, are consistent with changes in helix–helix interactions.

We then examined the double mutant Q207N/V232E-TM3/4 in which the potential polar partners are located in the sequence at the same positions as in V232D-TM3/4 (Q207 in TM3 and D232 in TM4). This mutant similarly migrates faster than V232D-TM3/4 (Fig. 1a, b). As shown in Fig. 4b and d, a striking similarity was observed between the $^{1}H–^{15}N$ HSQC 'Gly box' spectra of V232D- and Q207N/V232E-TM3/4, suggesting that the cross-peaks of their Gly residues can be correspondingly assigned, and that their global conformations likely correspond closely.

4. Discussion

4.1. Structural features of CFTR TM3/4 hairpins in micellar environments

While many studies addressing interhelical interactions in membranes have been carried out on homo-oligomeric TM helices [21,55], helical hairpin motifs of membrane proteins present ideal models for probing the less well-studied anti-parallel heterologous helix–helix interactions characteristic of polytopic membrane proteins. As noted here in Fig. 1a, b and throughout an extensive library of (>50) CFTR TM3/4 mutant hairpins studied earlier [19–23,53], gel shift migration behavior has been interpreted in terms of relative populations of open vs. closed hairpins, with faster migration indicated of higher populations of closed (globular) structures, and *vice versa*. While some mutants do contain a change in charge vs. WT, previous work from our laboratory has established that CFTR TM3/4 migration patterns are not simple functions of charge: (i) WT TM3/4 and the double mutant Q207L/V232D the same migration rates while V232D migrates significantly faster than WT [20]; (ii) Asp substitutions at 20 different positions along TM4 between residues 221 and 241 produce TM3/4 hairpins that migrate 3–12% faster than WT [22]; if introduction of a single negative charge was the dominating effect, all 20 mutants should display similar migration rates. In the present work, Q207N/V232E-TM3/4 migrates faster than TM3/4-V232D (Fig. 1b) although they each have one added negative charge vs. WT. In this context, it is interesting to note that while Glu pairings generally produce slowly migrating hairpins than Asp pairings with wild type Gln-207 when identically positioned TM4 mutants are compared [56], we nevertheless observed here (Fig. 1b) that Asn-207 pairings with Glu-231 and Glu-232 apparently produce tighter hairpins with a higher population of folded structures than corresponding Asp-231 and Asp-232 pairings. The latter observation suggests that the "reach" of the extra Glu methylene group in TM4 is a deciding factor in H-bond formation with suitably positioned TM3 polar partners.

Here we sought to extend the structural characterization of this lesion through high-resolution NMR studies of wild type and several mutant CFTR TM3/4 hairpin constructs expressed variously with ^{15}N and ^{13}C enrichment. While the gel experiments are performed in SDS, we performed the present NMR studies in PFO micelles as HSQC spectra in PFO presented the better dispersion and less peak broadening than the SDS HSQC spectra. An additional advantage for NMR studies is that PFO micelles (20 monomers) [54] are smaller than SDS micelles (>60 monomers), thus lowering the relative MW of the resulting protein/lipid particle. As well, we have previously shown from pyrene fluorescence studies that PFO is highly supportive of helix–helix tertiary interactions, and that in a series of LPC micelles comprising an alkyl chain length range of 8–18 carbons, octanoyl-PC (8 carbons) and nonanoyl-PC (9 carbons) – in addition to PFO (8 carbons) – display the greatest extent of interhelical packing [21]. It may be further noted that 'small' micelles have been employed for membrane protein structure determination; for example, the NMR solution structure of a peptide fragment derived from unprocessed mouse Doppel protein was resolved in DHPC, which has a smaller carbon chain length (C6) than PFO (C8) [57]. Indeed, when the protein is added to a detergent, its CMC and the aggregation number can be dramatically perturbed [58]. In cases where a TM helix is longer than can be accommodated by the free micelle, the properties of the helix should nevertheless primarily dictate the size of the protein–micelle complex since the exposure of helix hydrophobic surfaces would be thermodynamically unfavorable, and TM helices may flex, bend, or extend to satisfy hydrophobic mismatch [59].

Chemical shift data reported in Fig. 3 indicate that in PFO, a longer TM3 helix comprises residues G194 to A221 with a disruption of the helix around P205, and a shorter TM4 helix includes residues L227 to A238. Chemical shift deviation, amide hydrogen exchange, and a lack of NOEs for W202 to L206, provide further evidence for a discontinuity in the TM3 helix around P205. Studies by Akabas on the M3 membrane-spanning segment [13] similarly show a kink in this helix. We further observed that the turn (approximately S222 to G226) determined between TM3 and TM4 in the V232D-TM3/4 construct is shifted approximately six residues toward TM4 vs. the one predicted (W216 to Q220) in the original schematic presented for the wild type CFTR protein [6]. This may be a consequence, in part, of the cut-off point we chose in construct design; native residues 242–245 (RMMM), which are not indicated as an integral portion of TM4 segment by prediction, may well influence the length of the TM4 helix. This circumstance tends to 're-align' the TM3 and TM4 helices such that the TM4 D232 position is now within side chain-side chain interaction distance of the TM3 polar residue Glu-215. As well, we cannot rule out the possibility that polar mutations in TM4 may indeed seek out polar partners other than Q207, and thus it is the introduction of the mutation – not necessarily the PFO *per se* – that is skewing the helices. Whatever the origin of the experimentally-deduced inequality of length of TM3 *vs.* TM4, it is of course possible that the combination of the chosen construct sequences and the PFO micelle environment ultimately did not produce the specific TM3/TM4 interface that prevails in intact CFTR. Nevertheless, since all constructs were examined under identical conditions, comparisons among them are valid, and the interactions we detected for the participatory polar side chains likely typify those that occur *in vivo*.

Chemical shifts of indole N–H protons (visible in Fig. 2) are at the same frequency for all four constructs studied (data not shown); however, the Glu-215 may provide in each instance a viable 'polar partner' for each of D232, D231, and E232 introduced into TM4. Indeed, Glu–Glu side chain–side chain interactions have been noted in homodimers of designed Leu-rich peptides [60,61] and postulated in the TM segment of transforming mutants of the *neu* oncogene [62]. Here we observed that the E217 backbone amide ^{1}H (at 8.32 ppm) and ^{15}N (at 117.8 ppm) (Fig. 2) appears to be shifted in all three mutants vs. the WT (data not shown). This model would also 'bury' Q207 and Q237 in the PFO micelle, consistent with the observed lack of exchange of their carboxamide side chain protons with water.

4.2. Positional dependence of hairpin conformation on polar mutations

In performing a comparative analysis among the available hairpins, we focused on changes in the amide chemical shifts of Gly residues in the ^{1}H–^{15}N HSQC spectra among the various TM3/4 mutants in PFO micelles (Fig. 4). Gly residues in the tag regions (G3 and G23) displayed the same amide chemical shifts in the ^{1}H–^{15}N HSQC spectra of the WT and its mutants, confirming that the tags do not participate in the packing of the membrane spanning segments of TM3/4 under these conditions. Similarly, G194 present at the N-terminal end of TM3, is not affected by the V232D mutation (Fig. 4b). However, changes in the packing interface involved in helix–helix interactions are likely reflected in the observed changes of the remaining Gly residues G213 (located in the middle of TM3); G226 (in the turn); G228 (in the helical region of TM4); and G239 and G241 (located near the C-terminal region of TM4). In addition to these "Gly box" effects, chemical shift changes vs. WT in the amide proton dimension of virtually all of the residues in the V232D-TM3/4 spectrum, including A223, A225, and G226 from the turn, as well as W216, L218, L219, Q220, and A221 near the C-terminus of the TM3 helix (data not shown), confirming that the effect is not limited to immediate neighbors. These changes, in concert with results from migration rate data on SDS-PAGE, emphasize the fact that the interactions between helices differ in WT- vs. V232D-TM3/4. Such alteration in chemical shifts supports the notion that changes in interhelical packing represent the mutation-induced conformational response.

To address the proposition that the formation of a given helix–helix interface may be dominated by a positional dependence of a polar residue in TM4, the ^{1}H–^{15}N HSQC spectrum of I231D-TM3/4 in PFO micelles was acquired under identical conditions as WT-TM3/4 and V232D-TM3/4. The most drastic changes in the amide chemical shifts are observed for this mutant as reflected in the "Gly box" (Fig. 4c). The full amide chemical shift analysis of the ^{1}H–^{15}N HSQC shows that similarly to the V232D mutant, all TM4 amides – along with residues from W216 through A221 (C-terminus of TM3) and from S222 to G226 (turn) – are highly affected by the I231D mutation (not shown), suggesting that this mutation introduces significant changes in packing relative to WT protein. In contrast, the full ^{1}H–^{15}N HSQC spectra for V232D- and Q207N/V232E-TM3/4 exhibit striking similarities (not shown, but exemplified by the 'Gly box' comparison between Fig. 4 b and d), suggesting that these two mutants adopt similar conformations in the PFO micelle environment. The ^{1}H–^{15}N HSQC spectrum of this double mutant shows that similar to V232D-TM3/4 and I231D-TM3/4 mutants, the residues in TM4 along with some in TM3 and the turn are all highly affected vs. WT upon these mutations.

4.3. Structure of wild type vs. mutant TM3/4 hairpins of CFTR

Interhelical hydrogen bonding has been implicated as one of the main driving forces governing helix–helix packing in membranes [60,61,63]. Molecular dynamics simulations of WT TM3/4 vs. I231D-TM3/4 further support the view that a folded two-helix hairpin forms in a micellar environment, and that a side chain-side chain Q207-D231 H-bond provides additional stabilization for the folded state [64]. Although the NMR data reported here do not provide specific evidence for H-bond formation nor are sufficient for detailed structural characterization, one can speculate that the similarities in spectra of V232D and Q207N/V232E are the result of contacts between similar residues in the V232D mutant that can effectively be substituted by N207 and E232. Thus changes in packing/orientation of

helices relative to WT would be preserved in both mutants. Conversely, this model would predict that in the case of I231D, there must be a relative reorientation by 100° of one helix with respect to the other for participation of I231D in interhelical interactions *vs.* either V232D or Q207N/V232E.

In combination with earlier experimental investigations of TM3/4 hairpins [20–22], the present studies thus conjure a picture of mutant-dependent flexibility of transmembrane helical hairpin interfaces in the dynamic micellar environment. In such an environment, the secondary structure boundaries as well as interhelical packing might differ in order to reduce the free energy penalty arising from an apolar-to-polar mutation in the helical TM region. This could be achieved by alteration of helix–helix alignment for optimal adjustments of interhelical van der Waals packing that may involve rotation of one or both helices (depending on the location of the polar partners) — driven by the low dielectric environment of the membrane. Similar rotations of helical axes may be envisioned during folding steps of polytopic membrane proteins, where the corresponding sequential determinants for each helix–helix interface should prevail.

5. Conclusion

Features of the secondary structure of mutant V232D-TM3/4 helical hairpins of CFTR, along with comparisons to the WT and mutants I2231D and Q207N/V232E, have been determined using high resolution NMR spectroscopy. Although hairpin constructs have degrees of conformational freedom in SDS or PFO micellar environments that would not be available to the corresponding helices embedded in an intact CFTR TM domain, our results suggest that hairpin interfaces – and possibly helix boundaries – may vary as a function of the position of a non-native polar mutation (i.e., V232D vs. I231D in TM4), and thereby indicate the susceptibility of the native protein structure to a corresponding destiny. The overall findings provide a clear example as to how introduction of a polar mutation into a TM helix may, in principle, lead to distortion of native interfacial packing determinants in membrane proteins, with consequences that may lead to disease.

Acknowledgments

This work was supported, in part, by grants to C.M.D. from the Canadian Cystic Fibrosis Foundation (CCFF) and the Canadian Institutes of Health Research (CIHR). H.W. held a post-doctoral Award from the CIHR Strategic Training Program in 'Structural Biology of Membrane Proteins Linked to Disease'. M.Y.C. was the recipient of an award from the Hospital for Sick Children Research Training Committee. We are grateful to Lewis Kay and Peter Hwang for helpful discussions throughout the course of preparation of this manuscript.

References

[1] M.J. Welsh, L.C. Tsui, T.F. Boat, A.L. Beaudet, Cystic fibrosis, in: C.R. Scriver, A.L. Beaudet, W.S. Sly, et al., (Eds.), The metabolic and molecular basis of inherited disease, McGraw-Hill, New York, 1995, pp. 3799–3876.
[2] M.A. Gray, J.P. Winpenny, B. Verdon, H. McAlroy, B.E. Argent, Chloride channels and cystic fibrosis of the pancreas, Biosci. Rep. 15 (1995) 531–541.
[3] D.A. Gaillard, F. Carre-Pigeon, A. Lallemand, Normal vas deferens in fetuses with cystic fibrosis, J. Urol. 158 (1997) 1549–1552.
[4] L. Imundo, J. Barasch, A. Prince, Q. Al-Awqati, Cystic fibrosis epithelial cells have a receptor for pathogenic bacteria on their apical surface, Proc. Natl. Acad. Sci. U. S. A. 92 (1995) 3019–3023.
[5] J.M. Rommens, M.C. Iannuzzi, B. Kerem, M.L. Drumm, G. Melmer, M. Dean, R. Rozmahel, J.L. Cole, D. Kennedy, N. Hidaka, et al., Identification of the cystic fibrosis gene: chromosome walking and jumping, Science 245 (1989) 1059–1065.
[6] J.R. Riordan, J.M. Rommens, B. Kerem, N. Alon, R. Rozmahel, Z. Grzelczak, J. Zielenski, S. Lok, N. Plavsic, J.L. Chou, et al., Identification of the cystic fibrosis gene: cloning and characterization of complementary DNA, Science 245 (1989) 1066–1073.
[7] http://www.genet.sickkids.on.ca.
[8] K. Kunzelmann, ENaC is inhibited by an increase in the intracellular Cl(−) concentration mediated through activation of Cl(−) channels, Pflugers Arch. 445 (2003) 504–512.
[9] D.H. Hryciw, W.B. Guggino, Cystic fibrosis transmembrane conductance regulator and the outwardly rectifying chloride channel: a relationship between two chloride channels expressed in epithelial cells, Clin. Exp. Pharmacol. Physiol. 27 (2000) 892–895.
[10] A.P. Naren, E. Cormet-Boyaka, J. Fu, M. Villain, J.E. Blalock, M.W. Quick, K.L. Kirk, CFTR chloride channel regulation by an interdomain interaction, Science 286 (1999) 544–548.
[11] E.M. Schwiebert, M.M. Morales, S. Devidas, M.E. Egan, W.B. Guggino, Chloride channel and chloride conductance regulator domains of CFTR, the cystic fibrosis transmembrane conductance regulator, Proc. Natl. Acad. Sci. U. S. A. 95 (1998) 2674–2679.
[12] P. Linsdell, S.X. Zheng, J.W. Hanrahan, Non-pore lining amino acid side-chains influence anion selectivity of the human CFTR Cl(−) channel expressed in mammalian cell lines, J. Physiol. 512 (1998) 1–16.
[13] M. Cheung, M.H. Akabas, Locating the anion-selectivity filter of the cystic fibrosis transmembrane conductance regulator (CFTR) chloride channel, J. Gen. Physiol. 109 (1997) 289–299.
[14] M. Ramjeesingh, F. Ugwu, C. Li, S. Dhani, L.J. Huan, Y. Wang, C.E. Bear, Stable dimeric assembly of the second membrane-spanning domain of CFTR (cystic fibrosis transmembrane conductance regulator) reconstitutes a chloride-selective pore, Biochem. J. 375 (2003) 633–641.
[15] A.W. Partridge, A.G. Therien, C.M. Deber, Missense mutations in transmembrane domains of proteins: phenotypic propensity of polar residues for human disease, Proteins 54 (2001) 648–656.
[16] R.A. Melnyk, A.W. Partridge, C.M. Deber, Retention of native-like oligomerization states in transmembrane segment peptides: application to the *Escherichia coli* aspartate receptor, Biochemistry 40 (2001) 11106–11113.
[17] A.W. Partridge, R.A. Melnyk, D. Yang, J.U. Bowie, C.M. Deber, A transmembrane segment mimic derived from *Escherichia coli* diacylglycerol kinase inhibits protein activity, J. Biol. Chem. 278 (2003) 22056–22060.
[18] A. Rath, R.A. Melnyk, C.M. Deber, Evidence for assembly of small multidrug resistance proteins by a "two-faced" transmembrane helix, J. Biol. Chem. 281 (2006) 15546–15553.
[19] A.G. Therien, M. Glibowicka, C.M. Deber, Expression and purification of two hydrophobic double-spanning membrane proteins derived from the cystic fibrosis transmembrane conductance regulator, Protein Expr. Purif. 25 (2002) 81–86.
[20] A.G. Therien, F.E. Grant, C.M. Deber, Interhelical hydrogen bonds in the CFTR membrane domain, Nat. Struct. Biol. 8 (2001) 597–601.
[21] A.G. Therien, C.M. Deber, Interhelical packing in detergent micelles. Folding of a cystic fibrosis transmembrane conductance regulator construct, J. Biol. Chem. 277 (2002) 6067–6072.
[22] M.Y. Choi, L. Cardarelli, A.G. Therien, C.M. Deber, Non-native interhelical hydrogen bonds in the cystic fibrosis transmembrane conductance regulator domain modulated by polar mutations, Biochemistry 43 (2004) 8077–8083.
[23] M.Y. Choi, A.W. Partridge, C. Daniels, K. Du, G.L. Lukacs, C.M. Deber, Destabilization of the transmembrane domain induces misfolding in a

phenotypic mutant of cystic fibrosis transmembrane conductance regulator, J. Biol. Chem. 280 (2005) 4968–4974.
[24] W.C. Wigley, S. Vijayakumar, J.D. Jones, C. Slaughter, P.J. Thomas, Transmembrane domain of cystic fibrosis transmembrane conductance regulator: design, characterization, and secondary structure of synthetic peptides m1–m6, Biochemistry 37 (1998) 844–853.
[25] M. Katragadda, A. Chopra, M. Bennett, J.L. Alderfer, P.L. Yeagle, A.D. Albert, Structures of the transmembrane helices of the G-protein coupled receptor, rhodopsin, J. Pept. Res. 58 (2001) 79–89.
[26] J. Venkatraman, G.A. Nagana Gowda, P. Balaram, Structural analysis of synthetic peptide fragments from EmrE, a multidrug resistance protein, in a membrane-mimetic environment, Biochemistry 41 (2002) 6631–6639.
[27] K.D. Ridge, S.S. Lee, L.L. Yao, *In vivo* assembly of rhodopsin from expressed polypeptide fragments, Proc. Natl. Acad. Sci. U.S.A. 92 (1995) 3204–3208.
[28] N.P. Martin, L.M. Leavitt, C.M. Sommers, M.E. Dumont, Assembly of G protein-coupled receptors from fragments: identification of functional receptors with discontinuities in each of the loops connecting transmembrane segments, Biochemistry 38 (1999) 682–695.
[29] M.E. Girvin, V.K. Rastogi, F. Abildgaard, J.L. Markley, R.H. Fillingame, Solution structure of the transmembrane H+-transporting subunit c of the F1F0 ATP synthase, Biochemistry 37 (1998) 8817–8824.
[30] K. Oxenoid, H.J. Kim, J. Jacob, F.D. Sonnichsen, C.R. Sanders, NMR assignments for a helical 40 kDa membrane protein, J. Am. Chem. Soc. 126 (2004) 5048–5049.
[31] K.R. MacKenzie, J.H. Prestegard, D.M. Engelman, A transmembrane helix dimer: structure and implications, Science 276 (1997) 131–133.
[32] D. Ma, Z. Liu, L. Li, P. Tang, Y. Xu, Structure and dynamics of the second and third transmembrane domains of the human glycine receptor, Biochemistry 44 (2005) 8790–8800.
[33] E. Wallin, G. von Heijne, Genome-wide analysis of integral membrane proteins from eubacterial, archaean, and eukaryotic organisms, Protein Sci. 7 (1998) 1029–1038.
[34] K. Oxenoid, J.J. Chou, The structure of phospholamban pentamer reveals a channel-like architecture in membranes, Proc. Natl. Acad. Sci. U. S. A. 102 (2005) 10870–10875.
[35] S.C. Howell, M.F. Mesleh, S.J. Opella, NMR structure determination of a membrane protein with two transmembrane helices in micelles: MerF of the bacterial mercury detoxification system, Biochemistry 44 (2005) 5196–5206.
[36] J.H. Chill, J.M. Louis, C. Miller, A. Bax, NMR study of the tetrameric KcsA potassium channel in detergent micelles, Protein Sci. 15 (2006) 684–698.
[37] C.M. Franzin, X.M. Gong, K. Thai, J. Yu, F.M. Marassi, NMR of membrane proteins in micelles and bilayers: The FXYD family proteins, Methods 41 (2007) 398–408.
[38] F. Porcelli, B.A. Buck-Koehntop, S. Thennarasu, A. Ramamoorthy, G. Veglia, Structures of the dimeric and monomeric variants of magainin antimicrobial peptides (MSI-78 and MSI-594) in micelles and bilayers, determined by NMR spectroscopy, Biochemistry 45 (2006) 5793–5799.
[39] C. Fernandez, C. Hilty, G. Wider, P. Guntert, K. Wuthrich, NMR structure of the integral membrane protein OmpX, J. Mol. Biol. 336 (2004) 1211–1221.
[40] L.K. Tamm, F. Abildgaard, A. Arora, H. Blad, J.H. Bushweller, Structure, dynamics and function of the outer membrane protein A (OmpA) and influenza hemagglutinin fusion domain in detergent micelles by solution NMR, FEBS Lett. 555 (2003) 139–143.
[41] P.M. Hwang, W.Y. Choy, E.I. Lo, L. Chen, J.D. Forman-Kay, C.R. Raetz, G.G. Prive, R.E. Bishop, L.E. Kay, Solution structure and dynamics of the outer membrane enzyme PagP by NMR, Proc. Natl. Acad. Sci. U. S. A. 99 (2002) 13560–13565.
[42] P.M. Hwang, R.E. Bishop, L.E. Kay, The integral membrane enzyme PagP alternates between two dynamically distinct states, Proc. Natl. Acad. Sci. U. S. A. 101 (2004) 9618–9623.
[43] M. Wittekind, L. Mueller, HNCACB, a high-sensitivity 3D NMR experiment to correlate amide-proton and nitrogen resonances with the alpha-carbon and beta-carbon resonances in proteins, J. Magn. Reson., Ser. B 101 (1993) 201–205.
[44] S. Grzesiek, A. Bax, Correlating backbone amide and side-chain resonances in larger proteins by multiple relayed triple resonance NMR, J. Am. Chem. Soc. 114 (1992) 6291–6293.
[45] L.E. Kay, M. Ikura, R. Tschudin, A. Bax, Three-dimensional triple-resonance NMR spectroscopy of isotopically enriched proteins, J. Magn. Reson. 89 (1990) 496–514.
[46] T.M. Logan, E.T. Olejniczak, R.X. Xu, S.W. Fesik, A general method for assigning NMR spectra of denatured proteins using 3D HC(CO)NH-TOCSY triple resonance experiments, J. Biomol. NMR 3 (1993) 225–231.
[47] G.T. Montelione, B.A. Lyons, S.D. Emerson, M. Tashiro, An efficient triple resonance experiment using carbon-13 isotropic mixing for determining sequence-specific resonance assignments of isotopically-enriched proteins, J. Am. Chem. Soc. 114 (1992) 10974–10975.
[48] S.M. Pascal, D.R. Muhandiram, T. Yamazaki, J.D. Forman-Kay, L.E. Kay, Simultaneous acquisition of ^{15}N- and ^{13}C-edited NOE spectra of proteins dissolved in H_2O, J. Magn. Reson., Ser. B 103 (1994) 197–201.
[49] F. Delaglio, S. Grzesiek, G.W. Vuister, G. Zhu, J. Pfeifer, A. Bax, NMRPipe: a multidimensional spectral processing system based on UNIX pipes, J. Biomol. NMR 6 (1995) 277–293.
[50] B.A. Johnson, R.A. Blevins, NMRView: a computer program for the visualization and analysis of NMR data, J. Biomol. NMR 4 (1994) 603–614.
[51] G. Cornilescu, F. Delaglio, A. Bax, Protein backbone angle restraints from searching a database for chemical shift and sequence homology, J. Biomol. NMR 13 (1999) 289–302.
[52] C.M. Deber, C. Wang, L.P. Liu, A.S. Prior, S. Agrawal, B.L. Muskat, A.J. Cuticchia, TM Finder: a prediction program for transmembrane protein segments using a combination of hydrophobicity and nonpolar phase helicity scales, Protein. Sci. 10 (2001) 212–219.
[53] H. Wehbi, A. Rath, C.M. Deber, Role of the extracellular loop in the folding of a CFTR transmembrane helical hairpin, Biochemistry 46 (2007) 7099–7106.
[54] J.L. Lopez-Fontan, F. Sarmiento, P.C. Schulz, The aggregation of sodium perfluorooctanoate in water, Colloid Polym. Sci. 283 (2005) 862–871.
[55] R.A. Melnyk, A.W. Partridge, C.M. Deber, Transmembrane domain mediated self-assembly of major coat protein subunits from Ff bacteriophage, J. Mol. Biol. 315 (2002) 63–72.
[56] J.P. Dawson, R.A. Melnyk, C.M. Deber, D.M. Engelman, Sequence context strongly modulates association of polar residues in transmembrane helices, J. Mol. Biol. 331 (2003) 255–262.
[57] E. Papadopoulos, K. Oglecka, L. Maler, J. Jarvet, P.E. Wright, H.J. Dyson, A. Graslund, NMR solution structure of the peptide fragment 1–30, derived from unprocessed mouse doppel protein, in DHPC micelles, Biochemistry 45 (2006) 159–166.
[58] C.R. Sanders, K. Oxenoid, Customizing model membranes and samples for NMR spectroscopic studies of complex membrane proteins, Biochim. Biophys. Acta 1508 (2000) 129–145.
[59] P.L. Yeagle, M. Bennett, V. Lemaitre, A. Watts, Transmembrane helices of membrane proteins may flex to satisfy hydrophobic mismatch, Biochim. Biophys. Acta 1768 (2007) 530–537.
[60] F.X. Zhou, M.J. Cocco, W.P. Russ, A.T. Brunger, D.M. Engelman, Interhelical hydrogen bonding drives strong interactions in membrane proteins, Nat. Struct. Biol. 7 (2000) 154–160.
[61] H. Gratkowski, J.D. Lear, W.F. DeGrado, Polar side-chains drive the association of model transmembrane peptides, Proc. Natl. Acad. Sci. U. S. A. 98 (2001) 880–885.
[62] L.I. Chen, M.K. Webster, A.N. Meyer, D.L. Donoghue, Transmembrane domain sequence requirements for activation of the p185c-neu receptor tyrosine kinase, J. Cell Biol. 137 (1997) 619–631.
[63] J.P. Dawson, J.S. Weinger, D.M. Engelman, Motifs of serine and threonine can drive association of transmembrane helices, J. Mol. Biol. 316 (2002) 799–805.
[64] P.J. Bond, J. Holyoake, A. Ivetac, S. Khalid, M.S. Sansom, Coarse-grained molecular dynamics simulations of membrane proteins and peptides, J. Struct. Biol. 157 (2007) 593–605.